179
~~380~~
2-27-80

DR.755

ornl

OAK
RIDGE
NATIONAL
LABORATORY

UNION
CARBIDE

ORNL/TM-7074

MASTER

High n Ballooning Modes in Highly Elongated Tokamaks

C. H. Ar
Glenn Batemen

MASTER

MASTER

OPERATED BY
UNION CARBIDE CORPORATION
FOR THE UNITED STATES
DEPARTMENT OF ENERGY

ORNL/TM-7074
Dist. Category UC-20 g

Contract No. W-7405-eng-26

FUSION ENERGY DIVISION

HIGH n BALLOONING MODES IN HIGHLY ELONGATED TOKAMAKS

C. H. An
The University of Tennessee
Knoxville, Tennessee 37916

and

Glenn Bateman
School of Nuclear Engineering
Georgia Institute of Technology
Atlanta, Georgia 30332

Date Published - February 1980

NOTICE This document contains information of a preliminary nature. It is subject to revision or correction and therefore does not represent a final report.

Prepared by the
OAK RIDGE NATIONAL LABORATORY
Oak Ridge, Tennessee 37830
operated by
UNION CARBIDE CORPORATION
for the
DEPARTMENT OF ENERGY

CONTENTS

ABSTRACT

An analytic study of stability against high n ballooning modes in highly elongated axisymmetric plasmas is presented and compared with computational results.

From the equation for the marginal pressure gradient, it is found that the local shear plays an important role on the stability of elongated and shifted plasma, and that high elongation deteriorates the stability by decreasing the stabilizing effects of field line bending and local shear. The net contribution of the local shear to stability decreases with elongation and shift for strongly ballooning modes (eigenfunctions strongly localized near the outer edge of the toroidal flux surfaces) but increases for interchange modes (eigenfunctions more uniform along the flux surfaces).

The computational study of high n ballooning modes in a highly elongated plasma reveals that lowering the aspect ratio and broadening the pressure profile enhance the marginal beta for β_p less than unity but severely reduce the marginal beta for β_p larger than unity.

1. INTRODUCTION

The desirability of raising beta (the ratio of plasma pressure to magnetic pressure) in tokamaks has motivated the study of stability in elongated plasmas. Theoretical predictions indicate that high beta plasmas should be susceptible to ballooning modes. Analytic studies of ideal magnetohydrodynamic (MHD) ballooning modes have been made by Dobrott et al. [1] and Connor et al. [2]. In the limit of high toroidal mode number n, the problem reduces to a second order ordinary differential equation on each flux surface for the marginal stability condition. This analytic study is complementary to studies made by large two-dimensional (2-D) stability codes such as PEST [3], ERATO [4], and the initial value codes [5,6]. These analytic and computational studies provide information about the stability of high beta plasma in elongated tokamaks. However, because of the complicated interdependence of equilibrium parameters, their individual effects on stability for various equilibrium profiles are yet to be clarified. In order to study the high beta plasma more systematically and to understand and predict computational and experimental results correctly, it is important to know how each equilibrium parameter affects the stability.

This work is intended to clarify how high elongation and outward shift of a plasma affect the stabilizing and driving mechanisms of high n ballooning modes and to determine the most important equilibrium parameters for the stability of highly elongated tokamaks.

For the analytic part of this paper, large aspect ratio ($R_c/a \equiv \frac{1}{\varepsilon} \gg 1$) is assumed for the simplification of the problem, and high elongation ($b/a = \varepsilon^{-1/2} \gg 1$) is taken. This isolates the elongation effect from

other effects to elucidate the effect of elongation on the stability against high n ballooning modes. The ordinary differential equation for marginal stability against high n ballooning modes by Connor et al. [2] is used to construct a variational form of equation for the marginal pressure gradient. For equilibrium we follow the works done by Clarke et al. [7] and by Mizoguchi et al. [8] without further solving the Grad-Shafranov equilibrium equation. Expressions for the marginal pressure gradient as functions of equilibrium parameters are obtained using simple test functions in the variational form. These results are then compared with computational results using the ORNL BALOON code, and qualitative agreement is obtained.

The analytic result reveals that for the equilibria with reasonably high shear, high elongation deteriorates the stability by reducing the effects of field line bending and local shear (local helical pitch). Because the flux surfaces of elongated high beta plasmas are very distorted, stability strongly depends on the local shear rather than on the global shear. It is found that the stabilizing effect of local shear increases with plasma shift for an eigenfunction slowly varying along a poloidal flux line but decreases for an eigenfunction strongly localized near the outer edge of the plasma. The computational results show that the stability of a highly elongated plasma depends sensitively on the profile of the safety factor. Reducing the aspect ratio and increasing the breadth of the pressure profile are beneficial for high beta in highly elongated plasma only when poloidal beta is less than unity. The analytic results are used to interpret the computational results.

In Section 2, we construct a variational form for the marginal pressure gradient and express the marginal pressure gradient with several equilibrium parameters; the results are interpreted with respect to the local shear vs the distribution of eigenfunction and are compared with the computational results in Section 3. Detailed calculations for the local shear are given in the Appendix.

2. VARIATIONAL FORM OF EQUATION FOR MARGINAL STABILITY OF HIGH n BALLOONING MODES

An ordinary differential equation for marginal stability of high n ballooning modes by Connor et al. [2] is modified to a variational form to study the elongation effect on stability using a simple test function. The orthogonal flux coordinate system used is defined by the metric

$$(ds)^2 = \left(\frac{d\psi}{RB_p}\right)^2 + (JB_p d\chi)^2 + (Rd\zeta)^2 \tag{1}$$

Here ψ is a poloidal flux function, χ is a generalized poloidal angle, ζ is a toroidal angle, and J is Jacobian. The ordinary differential equation for marginal stability [2]

$$\frac{1}{J}\frac{d}{dy}\left\{\frac{1}{JR^2B_p^2}\left[1+\left(\frac{R^2B_p^2}{|\vec{B}|}\int\frac{\partial\nu}{\partial\psi}\,dy\right)^2\right]\frac{dF}{dy}\right\}$$

$$+\frac{2}{RB_p}\frac{dP}{d\psi}\left(K_n - \frac{I(\psi)RB_p^2}{|\vec{B}|^2}K_s\int^y\frac{\partial\nu}{\partial\psi}\,dy\right)F = 0 \tag{2}$$

is used to construct a variational form, leading to the stability condition

$$\frac{\int_{-\infty}^{\infty}\frac{1}{JR^2B_p^2}\left\{1+\left[\frac{R^2B_p^2}{|\vec{B}|}\int^y\left(\frac{\partial\nu}{\partial\psi}\right)_y dy\right]^2\right\}\left|\frac{dF}{dy}\right|^2 dy}{-\int_{-\infty}^{\infty}\frac{2J}{RB_p}\left[K_n - \frac{I(\psi)RB_p^2}{|\vec{B}|^2}K_s\int^y\left(\frac{\partial\nu}{\partial\psi}\right)_y dy\right]|F|^2\,dy} > \left|\frac{dP}{d\psi}\right| \tag{3}$$

Here K_n, K_s are normal and geodesic curvature defined as

$$K_n = \frac{\nabla\psi}{|\nabla\psi|} \cdot (\hat{B} \cdot \nabla)\hat{B}$$

$$K_s = \frac{\nabla\psi \times \vec{B}}{|\nabla\psi||\vec{B}|} \cdot (\hat{B} \cdot \nabla)\hat{B} \tag{4}$$

B_p is poloidal B field, $I(\psi) = RB_t$ (B_t is toroidal B field), and F is a test function corresponding to $RB_p\xi_\psi$ where ξ_ψ is the component of the displacement normal to the flux surface. The generalized poloidal angle χ is replaced with variable y whose range is from $-\infty$ to $+\infty$ [2]. ν is defined as

$$\nu = \frac{JB_t}{R} \tag{5}$$

For equilibrium, we follow the work done by Clarke and Sigmar [7] and Mizoguchi et al. [8]. Several assumptions are made to simplify the problem and isolate the effects of each equilibrium parameter from other effects. First, flux surfaces are taken to be vertically elongated ellipses, each with different elongation and shift; second, the aspect ratio is taken to be very large so that $a/R_c \equiv \varepsilon \ll 1$; third, the elongation e ($\equiv b/a$) is taken to be large as order of $e \sim 0(\varepsilon^{-1/2})$; fourth, flux function is assumed to be more or less parabolic.

The assumption of elliptic cross section of each flux surface makes ψ a function of $\bar{\rho}^2$, i.e.,

2. VARIATIONAL FORM OF EQUATION FOR MARGINAL STABILITY OF HIGH n BALLOONING MODES

An ordinary differential equation for marginal stability of high n ballooning modes by Connor et al. [2] is modified to a variational form to study the elongation effect on stability using a simple test function. The orthogonal flux coordinate system used is defined by the metric

$$(ds)^2 = \left(\frac{d\psi}{RB_p}\right)^2 + (JB_p d\chi)^2 + (Rd\zeta)^2 \tag{1}$$

Here ψ is a poloidal flux function, χ is a generalized poloidal angle, ζ is a toroidal angle, and J is Jacobian. The ordinary differential equation for marginal stability [2]

$$\frac{1}{J}\frac{d}{dy}\left\{\frac{1}{JR^2B_p^2}\left[1+\left(\frac{R^2B_p^2}{|\vec{B}|}\int\frac{\partial\nu}{\partial\psi}dy\right)^2\right]\frac{dF}{dy}\right\}$$

$$+\frac{2}{RB_p}\frac{dP}{d\psi}\left(K_n - \frac{I(\psi)RB_p^2}{|\vec{B}|^2}K_s\int^y\frac{\partial\nu}{\partial\psi}dy\right)F = 0 \tag{2}$$

is used to construct a variational form, leading to the stability condition

$$\frac{\int_{-\infty}^{\infty}\frac{1}{JR^2B_p^2}\left\{1+\left[\frac{R^2B_p^2}{|\vec{B}|}\int^y\left(\frac{\partial\nu}{\partial\psi}\right)_y dy\right]^2\right\}\left|\frac{dF}{dy}\right|^2 dy}{-\int_{-\infty}^{\infty}\frac{2J}{RB_p}\left[K_n - \frac{I(\psi)RB_p^2}{|\vec{B}|^2}K_s\int^y\left(\frac{\partial\nu}{\partial\psi}\right)_y dy\right]|F|^2 dy} > \left|\frac{dP}{d\psi}\right| \tag{3}$$

Here K_n, K_s are normal and geodesic curvature defined as

$$K_n = \frac{\nabla\psi}{|\nabla\psi|} \cdot (\hat{B} \cdot \nabla)\hat{B}$$

$$K_s = \frac{\nabla\psi \times \vec{B}}{|\nabla\psi|\,|\vec{B}|} \cdot (\hat{B} \cdot \nabla)\hat{B} \tag{4}$$

B_p is poloidal B field, $I(\psi) = RB_t$ (B_t is toroidal B field), and F is a test function corresponding to $RB_p\xi_\psi$ where ξ_ψ is the component of the displacement normal to the flux surface. The generalized poloidal angle χ is replaced with variable y whose range is from $-\infty$ to $+\infty$ [2]. ν is defined as

$$\nu = \frac{JB_t}{R} \tag{5}$$

For equilibrium, we follow the work done by Clarke and Sigmar [7] and Mizoguchi et al. [8]. Several assumptions are made to simplify the problem and isolate the effects of each equilibrium parameter from other effects. First, flux surfaces are taken to be vertically elongated ellipses, each with different elongation and shift; second, the aspect ratio is taken to be very large so that $a/R_c \equiv \varepsilon \ll 1$; third, the elongation e ($\equiv b/a$) is taken to be large as order of $e \sim O(\varepsilon^{-1/2})$; fourth, flux function is assumed to be more or less parabolic.

The assumption of elliptic cross section of each flux surface makes ψ a function of $\overline{\rho}^2$, i.e.,

$$\psi = S(\overline{\rho}^2)$$

$$\overline{\rho}^2 = x^2 + \frac{1}{e^2} z^2 \tag{6}$$

with

$$x = R - R_c - \delta(\psi)$$

$$e = b/a \tag{7}$$

where e is the elongation, $\delta(\psi)$ is the shift of a flux surface ψ, and R_c is the geometric center of the plasma. (See Fig. 1.) ψ is assumed to increase with the increase of minor radius $a(\psi)$. B_p, B_t, and $q(\psi)$ are calculated from the relations $RB_p = |\nabla\psi|$, $RB_t = I(\psi)$, and $q(\psi) = \frac{1}{2\pi} \oint \frac{JB_t}{R} d\chi$, respectively. If we use elliptic angle θ on a flux surface ψ such as

$$x = a(\psi) \cos\theta$$

$$z = b(\psi) \sin\theta \tag{8}$$

B_p, B_t are expressed with (ψ,θ,ζ) by neglecting terms with order higher than $O(\epsilon^2)$,

$$B_p \cong \frac{2\dot{S}a}{R_c} \left(\cos^2\theta + \frac{1}{e^2} \sin^2\theta\right)^{1/2} \left[1 - \left(\frac{a}{R_c} + 2\delta'\dot{S}a\right) \cos\theta - \frac{2e'}{e} \dot{S}a^2 \sin^2\theta\right]$$

$$B_t \cong \frac{2\dot{S}q(\psi)}{e} \left(1 - \frac{2e'}{e} \dot{S}a^2 - \frac{a \cos\theta}{R_c}\right) \tag{9}$$

where

$$\dot{S} \equiv \frac{dS}{d\overline{\rho^2}} , \quad e' \equiv \frac{de}{d\psi} , \quad \text{and} \quad \delta' \equiv \frac{d\delta}{d\psi}$$

The poloidal flux function ψ is assumed minimum at the magnetic axis and maximum at the plasma edge. The transformation of the coordinate system from any orthogonal flux coordinate system (ψ,χ,ζ) to the nonorthogonal flux coordinate system (ψ,θ,ζ) in Eq. (3) can be simply done by noticing that once χ is chosen on a given flux surface it is then determined on all the flux surfaces for a given equilibrium by the equation

$$-\frac{R^2}{J}\frac{\partial}{\partial\psi}\left(JB_p^2\right) = R^2P' + II'(\psi) \tag{10}$$

and the relations

$$\begin{aligned} J &= \frac{ae}{B_p}\left(\cos^2\theta + \frac{1}{e^2}\sin^2\theta\right)^{1/2}\left(\frac{\partial\theta}{\partial\chi}\right)_\psi \\ d\chi &= \left(\frac{\partial\chi}{\partial\theta}\right)_\psi d\theta \end{aligned} \tag{11}$$

However, the transformation of the coordinate system in $\int\left(\frac{\partial\nu}{\partial\psi}\right)_\chi d\chi$ is rather involved because $\left(\frac{\partial\nu}{\partial\psi}\right)_\chi \neq \left(\frac{\partial\nu}{\partial\psi}\right)_\theta$. Direct calculation should be done by expressing ν with (ψ,θ) and using Eq. (11); the detailed calculation is given in the Appendix. The result, as a function of (ψ,θ,ζ), is

$$\int^y \left(\frac{\partial\nu}{\partial\psi}\right)_y dy = S_1\theta + S_2\frac{\tan\theta}{1 + (1/e^2)\tan^2\theta} + \sigma \tag{12}$$

S_1, S_2 are zero order coefficients and stand for global shear and a geometric effect (or residual shear [9]), respectively. σ is a first order correction and is

$$\sigma \equiv S_3 \sin\theta + S_4 \sin 2\theta + S_5 \, e \tan^{-1}\left(\frac{1}{e}\tan\theta\right) \tag{13}$$

The coefficients S_1, S_2,... , S_5 are shown in the Appendix. The term $\int\left(\frac{\partial\nu}{\partial\psi}\right)_y dy$ plays an important role in determining the stability for highly elongated plasmas. Explanation about the meaning of this term will be given later.

The test function is chosen for simplicity of the calculation while giving a severe restriction for stability. To meet the requirement we choose between two simple test functions defined as follows:

$$F_1(\theta) = \begin{cases} 1 + \cos\theta & -\pi \leq \theta \leq \pi \\ 0 & \text{elsewhere} \end{cases}$$

$$F_2(\theta) = \begin{cases} 1 + \cos 2\theta & -\frac{\pi}{2} \leq \theta \leq \frac{\pi}{2} \\ 0 & \text{elsewhere} \end{cases} \tag{14}$$

These test functions would give optimistic stability criteria because of the finite range of θ.

For the test function $F_1(\theta)$, the marginal pressure gradient is $\left|\frac{dP}{d\bar{\rho}^2}\right|$,

$$\left|\frac{dP}{d\bar{\rho}^2}\right|_1 < \left(\frac{\dot{S}^2}{R_c \dot{a}}\right) \frac{\left\{\frac{1}{e} + \frac{(\dot{S}a^2)^2}{2\pi}\left[10\left(\frac{q'}{q}\right)^2 + \frac{2.4}{(\dot{S}a^2)^2} + 2.4\left(\frac{q'}{q}\right)\frac{1}{\dot{S}a^2} + \Delta_1\right]\right\}}{1 + \frac{5}{3}\dot{S}a^2\left(\frac{q'}{q}\right) + \Delta_2} \tag{15}$$

It is compared with $\left|\frac{dP}{d\bar{\rho}^2}\right|_2$ for the test function $F_2(\theta)$,

$$\left|\frac{dP}{d\bar{\rho}^2}\right|_2 < \left(\frac{8\pi\dot{S}^2}{5R_c a}\right) \frac{\left\{\frac{1}{e^2} + \frac{(\dot{S}a^2)^2}{2\pi}\left[1.6\left(\frac{q'}{q}\right)^2 + \frac{0.8}{(\dot{S}a^2)^2} - 2.1\left(\frac{q'}{q}\right)\frac{1}{\dot{S}a^2} + \Delta_3\right]\right\}}{1 + 0.4\,\dot{S}a^2\left(\frac{q'}{q}\right) + \Delta_4} \tag{16}$$

Here Δ_1, Δ_2, Δ_3, and Δ_4 are correction terms with toroidicity, shift, and variation of inner elongation. Their expressions will be shown and their effects will be discussed later.

An appropriate test function is chosen by comparing $\left|\frac{dP}{d\bar{\rho}^2}\right|_1$ and $\left|\frac{dP}{d\bar{\rho}^2}\right|_2$ for equilibria with different shear. For the equilibria with reasonably high shear, i.e., $\left(\frac{q'}{q}\right)\dot{S}a^2 \gg 1$ and $1/e^2 \cong 0.1$, it is found that $\left|\frac{dP}{d\bar{\rho}^2}\right|_2 < \left|\frac{dP}{d\bar{\rho}^2}\right|_1$. In this case, the test function $F_2(\theta)$ is an appropriate test function because it more nearly minimizes the variational form. But for the equilibria with very low shear, i.e., $\left(\frac{q'}{q}\right) \times \frac{1}{\dot{S}a^2} \ll 1$, $F_1(\theta)$ is an appropriate one because $\left|\frac{dP}{d\bar{\rho}^2}\right|_1 < \left|\frac{dP}{d\bar{\rho}^2}\right|_2$. The dependences of eigenfunctions on shear are shown in Figs. 2 and 3 using the ORNL BALOON code. Eigenfunctions are plotted as a function of poloidal arc length 3.5 times around the poloidal cross section (Fig. 2) and 0.5 times around the poloidal cross section (Fig. 3) with high shear (a) and low shear (b) of elongation 3. Figure 3 shows that test functions $F_1(\theta) = 1 + \cos\theta$ and $F_2(\theta) = 1 + \cos 2\theta$ in Eq. (14) are good approximations for low shear and for high shear, respectively. Because usual tokamaks have relatively high shear, we concentrate on the marginal pressure gradient $\left|\frac{dP}{d\bar{\rho}^2}\right|_2$ obtained from the second test function, Eq. (16), for further study.

3. INTERPRETATION FOR STABILITY

The stability of highly elongated elliptic plasmas with relatively high shear is expressed with Eq. (16). The first parenthesis on the right side of Eq. (16) shows the effects of toroidicity ($\sim 1/R_c$) and poloidal flux profile ($\sim \dot{S}^2$) on the marginal pressure gradient. The numerator of Eq. (16) corresponds to a stabilizing mechanism and the denominator corresponds to a driving mechanism. The driving mechanism has two effects; the first comes from normal curvature and the other from geodesic curvature. There are two effects in the stabilizing mechanism: the field line bending effect, which decreases as $1/e^2$ with elongation e, and the local shear effect [9]. The local shear effect has three terms: global shear $(q'/q)^2$, a geometric effect $\frac{1}{(\dot{S}a^2)^2}$, and the combined effect of global shear and geometry $\left(\frac{q'}{q}\right)\frac{1}{\dot{S}a^2}$. The last two terms, $\frac{1}{(\dot{S}a^2)^2}$ and $\left(\frac{q'}{q}\right)\frac{1}{\dot{S}a^2}$, do not have correspondence to the stabilizing mechanism in circular tokamaks with concentric flux configurations [10]. The term $\frac{1}{(\dot{S}a^2)^2}$ contributes to stabilization and is independent of global shear. The term $\left(\frac{q'}{q}\right)\frac{1}{\dot{S}a^2}$ contributes to a destabilization for the usual tokamak condition ($q' > 0$) and the destabilization is large compared with other stabilization terms in local shear effect. The reduction of the field line bending effect as $1/e^2$ and additional terms $\frac{1}{(\dot{S}a^2)^2}$ and $\left(\frac{q'}{q}\right)\frac{1}{\dot{S}a^2}$ in local shear effect are characteristics of stability in highly elongated plasmas.

The appearance of these additional effects can be understood by considering the term $\left.\frac{\partial \nu}{\partial \psi}\right|_{\chi}$ in Eq. (2) for an elliptically elongated

cylinder. It is found that the term $\left.\frac{\partial \nu}{\partial \psi}\right|_{\chi}$ is proportional to local shear and a local intersection angle between two field lines on adjacent flux surfaces during an interchange of plasma.

The local shear [9] expressed with orthogonal flux coordinates as

$$\frac{\vec{B} \times \nabla\psi \cdot \nabla \times (\vec{B} \times \nabla\psi)}{|\nabla\psi|^4} = -\frac{\nu'}{J} \tag{17}$$

where J is the Jacobian and ν' appears in Eqs. (3) and (11). Greene and Johnson [9] expressed this local shear in Hamada coordinates [11,12] and found that the local shear consists of two parts, global and residual shear.

It will now be shown that the term ν'/J is also proportional to a local intersection angle of two field lines on adjacent flux surfaces during an interchange of plasma.

The local intersection angle is calculated by assuming that plasma motion has only a perpendicular component to a flux surface. In an elliptic cylinder the angle α_1 between a field line on ψ and the z axis of the cylinder is (see Fig. 4)

$$\tan \alpha_1 = \frac{B_p(\psi,\chi)}{B_t(\psi,\chi)} \tag{18}$$

The angle α_2 between a field line moving from $\psi - \delta\psi$ to ψ and the z axis is

$$\tan \alpha_2 = \frac{B_p(\psi - \delta\psi, \chi) + \dfrac{\vec{B}_p \cdot (\vec{\xi} \cdot \nabla)\vec{B}}{|\vec{B}_p|} + B_{1P}}{B_t(\psi - \delta\psi, \chi) + \dfrac{\vec{B}_t \cdot (\vec{\xi} \cdot \nabla)\vec{B}}{|\vec{B}_t|} + B_{1t}} \tag{19}$$

by adopting a Lagrangian description [13] of the plasma motion. Here B_{1P} and B_{1t} are poloidal and toroidal components of $\vec{B}_1 = \nabla \times (\vec{\xi} \times \vec{B})$. By neglecting displacement parallel to the flux surface and using Eqs. (18) and (19), we get an intersection angle $\delta\alpha$

$$\delta\alpha \cong \tan(\alpha_1 - \alpha_2) = \left(|\nabla\psi| \frac{\vec{\xi} \cdot \nabla\psi}{B_t^2}\right) \frac{\nu'}{J} \tag{20}$$

assuming $\delta\alpha = \alpha_1 - \alpha_2 \ll 1$. Equation (23) shows that $\frac{\nu'}{J}$ is proportional to the local intersection angle; consequently, local shear is proportional to the local intersection angle.

Next, we consider ν' evaluated for a special geometry, i.e., elliptically elongated toroid with very large aspect ratio, to illustrate the effects of elongation and shift on the local shear and consequently on the stability. Using Eqs. (5), (9), and (10) and taking the most important term, we get

$$\nu = q\left(\frac{\partial\theta}{\partial\chi}\right)_\psi \tag{21}$$

The derivative of ν with ψ is

$$\left(\frac{\partial\nu}{\partial\psi}\right)_\chi = q\left(\frac{\partial\theta}{\partial\chi}\right)_\psi \left\{\left(\frac{q'}{q}\right) + \left(\frac{\partial\chi}{\partial\theta}\right)_\psi \frac{\partial}{\partial\psi}\left[\left(\frac{\partial\theta}{\partial\chi}\right)_\psi\right]_\chi\right\} \tag{22}$$

Judging from the above consideration about the meaning of the term $\left(\frac{\partial \nu}{\partial \psi}\right)_\chi$, the last term of Eq. (22) is proportional to the residual shear, which has a strong dependence on the geometry of poloidal flux surfaces.

Consider the physical meaning of $\frac{\partial}{\partial \psi}\left[\left(\frac{\partial \theta}{\partial \chi}\right)_\psi\right]_\chi$ in an effort to explain the geometric effect on the stability. Figure 5 shows two adjacent elliptic flux surfaces, $\psi - \delta\psi$ and ψ. A generalized poloidal angle χ is determined exactly the same as an elliptic angle θ on one particular flux surface $\psi - \delta\psi$. The deviation of these two angles is shown in the flux surface ψ. Figure 6 shows the relations between χ and θ on different flux surfaces. Because of the geometric effect, θ changes slowly with χ near $\theta = 0$ but changes rapidly near $\theta = \pm\pi/2$. Figure 6 snows how $\left(\frac{\partial \theta}{\partial \chi}\right)_\psi$ changes for different adjacent flux surfaces, i.e., it measures $\frac{\partial}{\partial \psi}\left[\left(\frac{\partial \theta}{\partial \chi}\right)_\psi\right]_\chi$. Because the term $\frac{\partial}{\partial \psi}\left[\left(\frac{\partial \theta}{\partial \chi}\right)_\psi\right]_\chi$ (or residual shear) is negative near $\theta = 0$ but positive near $\theta = \pm\pi/2$, the local shear decreases near $\theta = 0$ but increases near $\theta = \pm\pi/2$ for the usual tokamak condition $q' > 0$. Therefore, if an eigenfunction is strongly localized near $\theta = 0$, then the negative contribution of the residual shear near $\theta = 0$ to the local shear dominates the positive contribution near $\theta = \pm\pi/2$, resulting in a decrease of the local shear effect and the negative sign of the term $2.1(q'/q)\frac{1}{\hat{s}a^2}$ in the numerator of Eq. (16). On the other hand, if the eigenfunction is broadly distributed along a poloidal flux line, then the positive contribution of the residual shear near $\theta = \pm\pi/2$ dominates the negative contribution near $\theta = 0$. That is why we get a positive sign of the term $2.4(q'/q)\frac{1}{\hat{s}a^2}$ in the numerator of Eq. (15). The terms

$\frac{2.4}{(\dot{S}a^2)^2}$ and $\frac{0.8}{(\dot{S}a^2)^2}$ in Eqs. (15) and (16), respectively, come from the residual shear effect only. It is found that the elongation effect comes from the residual shear and the distribution of eigenfunctic along a poloidal flux line.

The effects of residual shear are not confined only to the elongation of the plasma cross section.

Any distortion of plasma cross section — D shapeness, shift, elongation, etc. — can change the effect of the residual shear on stability. The effects of shift and variable elongation of inner flux surface are studied by considering the correction terms Δ_3 and Δ_4; the effect of D shapedness is not studied in this paper.

The correction terms Δ_3 and Δ_4 in Eq. (16) are given as follows:

$$\Delta_3 \equiv \left(\frac{q'}{q}\right)^2 \left(\frac{2.8}{e^2} - 3.4\,\frac{e'}{e}\,\dot{S}a^2 - 1.9\,\frac{a}{R_c} + 0.6\dot{S}\delta' a\right)$$

$$+ \left(\frac{q'}{q}\right)\frac{1}{\dot{S}a^2}\left(\frac{6.9}{e^2} + 5.1\,\frac{e'}{e}\,\dot{S}a^2 + 0.6\,\frac{a}{R_c} + 4.1\dot{S}\delta' a\right) \qquad (23)$$

$$+ \frac{1}{(\dot{S}a^2)^2}\left(\frac{-3.4}{e^2} - 1.6\,\frac{e'}{e}\,\dot{S}a^2 + 0.5\,\frac{a}{R_c} - 2.7\dot{S}\delta' a\right)$$

$$\Delta_4 \equiv 0.8\,\frac{a}{R_c} + 3.3\dot{S}\delta' a - 0.2\,\frac{e'}{e}\,\dot{S}a^2$$

$$+ \dot{S}a^2\left(\frac{q'}{q}\right)\left(0.6\,\frac{e'}{e}\,\dot{S}a^2 + 1.2\dot{S}\delta' a + 0.3\,\frac{a}{R_c}\right) \qquad (24)$$

Δ_3 shows how the stabilization of the local shear is affected by shift, aspect ratio, and elongation.

First, we consider the effect of shift. Because the flux function ψ is assumed to be maximum at the plasma edge and minimum at the magnetic axis (Section 2), $\dot{S}\delta'a$ is negative for the outward shift of the plasma. The overall effect of shift in Δ_3 is destabilizing for high shear $\left[\left(\frac{q'}{q}\right)\dot{S}a^2 > 1\right]$. The effect of shift on the stability can be related to the effect of residual shear by considering the term $\frac{\partial}{\partial\psi}\left[\left(\frac{\partial\theta}{\partial\chi}\right)_\psi\right]_\chi$ in Eq. (22) again. We find that for shifted flux surfaces, $\frac{\partial}{\partial\psi}\left[\left(\frac{\partial\theta}{\partial\chi}\right)_\psi\right]_\chi$ is negative at $0 \leq \theta < \pi/2$ but positive at $\pi/2 < \theta \leq \pi$. Therefore, if the eigenfunction is strongly localized near $\theta = 0$, then the negative contribution of $\frac{\partial}{\partial\psi}\left[\left(\frac{\partial\theta}{\partial\chi}\right)_\psi\right]_\chi$ to the local shear dominates the positive contribution. For this reason, shift reduces the stabilizing force for the eigenfunction strongly localized near $\theta = 0$ [such as $F_2(\theta)$ in Eq. (14)]. However, shift increases the stabilizing force if the eigenfunction varies slowly along the poloidal flux line [such as $F_1(\theta)$ in Eq. (14)].

The effect of variation of the elongation of the inner flux surfaces can also be explained in terms of residual shear. When the inner flux surfaces are less elongated than the outer flux surfaces, the local shear is reduced near $\theta = 0$ and increased near $\theta = \pi/2$. Hence, according to the same argument used above, those perturbations strongly localized near $\theta = 0$ are destabilized.

The overall destabilizing effects of shift and variation of inner elongation using eigenfunction $F_2(\theta)$ and shear $(q'/q)\dot{S}a^2 > 1$, are shown in Δ_3 of Eq. (26).

The correction term Δ_4 of Eq. (24) consists of two parts; the first three terms are due to normal curvature and the last three terms are due to geodesic curvature. Because the driving force by geodesic curvature is proportional to the local shear, shift reduces this driving force for equilibria with high shear $[(q'/q)\hat{S}a^2 > 1]$. However, the stabilizing effect of shift in the driving force Δ_4 does not exceed the destabilizing effect in the stabilizing force Δ_3. The interpretation of the effects of shift and the variation of inner elongation on the driving force is not as simple as that of the effects on the stabilizing force because of the curvature effect. Further detailed interpretation of the effects of shift and distortion of flux surfaces requires a more correct test function and a better approximation to calculate equilibrium profiles and the marginal pressure gradient.

The analytic results are compared with the computational results using the ORNL BALOON code for various equilibria with elongation $(b/a)w = 3$. The marginal curves are plotted in $\beta \left[\equiv \frac{\langle P \rangle}{(1/2)B_t^2} \right]$ and

$$\beta_p \left[\equiv \frac{\langle P \rangle}{\left(\frac{1}{2}\right)\oint_c B_p^2 d\ell / \oint_c d\ell} \right]$$

parameter space for various $q(\psi)$ profiles and aspect ratios. Figures 7-9 show how stability depends on shear, aspect ratio, and the breadth of pressure profile for plasma with high elongation. From Fig. 7, it is seen that stability sensitively depends on the profile of $q(\psi)$ because shear is a major stabilizing mechanism for the highly elongated plasma. The value of $q'(\psi)$ $\left(\equiv \frac{dq}{d\psi}\right)$ for curve 1 decreases to zero as flux surfaces

become close to the plasma edge; $q'(\psi)$ for the other two curves remains constant. The rapid drop of marginal beta for the curve 1 with β_p is due to the fact that as β_p increases the most unstable region of flux surfaces moves to the plasma edge, where global shear (q') decreases to zero and where the stabilizing effect of residual shear due to the plasma shift is negligible.

Figure 8 shows that the low aspect ratio plasma has higher marginal beta for lower β_p but lower marginal beta for higher β_p. The effect of aspect ratio shown in Fig. 8 can be understood from the terms of a/R_c in Δ_3 and Δ_4. The overall toroidicity effects (a/R_c) in Δ_3 and Δ_4 are destabilizing; i.e., lower aspect ratio reduces the stabilizing force and increases the driving force in Δ_3 and Δ_4, respectively. This destabilizing effect of toroidicity in Δ_3 and Δ_4 competes with the stabilizing effect of a/R_c in the first parenthesis of Eq. (16).

The effect of pressure profile on marginal beta is straightforward to understand. Broadening the pressure profile enhances the marginal beta for β_p less than unity but reduces the marginal beta for β_p larger than unity. Because the pressure gradient near the plasma edge increases with the breadth of pressure profile and plasma shift, marginal beta of the highly elongated plasma with broader pressure profile drops more rapidly with β_p, as shown in Fig. 9.

The convergence studies with finer grids show no appreciable difference between the results of a grid size 33 x 65, which is most often used, and a 65 x 65 grid. However, Fig. 10 shows noticeable differences between the results with different intervals of integration variable y of Eq. (2). The intervals of integration variables y are 3.5

and 28.5 times around the cross section, and q_a of the solid curves and of the dotted curves is 1 and 1.5, respectively. As the most unstable region of flux surface is closer to the magnetic axis (interchange instability), the difference of the results becomes more significant. The marginal betas of dotted curves are scaled down as $\beta = \beta_1/(1.5)^2$, where β_1 and β are marginal betas with $q_a = 1$ and 1.5, respectively. The convergence study with a different integration angle indicates also that the Mercier stability criterion [14,15] cannot be generated with the computational study, mainly due to the computational error near the magnetic axis.

4. CONCLUSION

In summary, the stability of highly elongated tokamaks depends on two effects: one is the field line bending effect which decreases as $1/e^2$ with elongation $e = b/a$; the other is the local shear effect in a rather complicated manner. The overall contribution of the local shear to the stability of a plasma depends on the global shear and the elongation in such a way that large global shear and high elongation reduce the stabilizing effect of the local shear. Because the residual shear comes from the geometric configuration of flux surfaces, the effect on the stability of shaping the cross section can also be understood with the local (or residual) shear. From the computational study it is found that high elongation, low aspect ratio, and broad pressure profile enhance the marginal beta value for β_p less than unity but severely reduce the marginal beta for β_p larger than unity.

ACKNOWLEDGMENTS

The authors acknowledge Dr. D. B. Nelson for his valuable comments and discussions.

This research was sponsored jointly by the University of Tennessee under contract DOE EY-76-S-052598 and the Office of Fusion Energy (ETM), U.S. Department of Energy, under contract W-7405-eng-26 with the Union Carbide Corporation.

APPENDIX

The calculation of $\int^{\chi} \left(\frac{\partial \nu}{\partial \psi}\right)_{\chi} d\chi$

Because the coordinate system we have used is not an orthogonal coordinate system and $\left(\frac{\partial \nu}{\partial \psi}\right)_{\chi}$ is different from $\left(\frac{\partial \nu}{\partial \psi}\right)_{\theta}$, we have to calculate the integral $\int \left(\frac{\partial \nu}{\partial \psi}\right)_{\chi} d\chi$ in a way which is independent of the coordinate system. Using $\nu = \frac{JB_t}{R}$ and $d\ell_p = JB_p d\chi$, $\int^{\chi} \left(\frac{\partial \nu}{\partial \psi}\right)_{\psi} d\chi$ can be changed to an expression independent of the coordinate system as

$$\int \left(\frac{\partial \nu}{\partial \psi}\right)_{\chi} d\chi = \int d\ell_p \left[\frac{I(\psi)J_t}{(RB_p)^3} + \frac{B_p I'(\psi)}{(RB_p)^2} - \frac{2B_p I'(\psi)}{(RB_p)^3} \frac{\partial}{\partial \psi} (RB_p)\right] \qquad (A.1)$$

Here J_t is the toroidal current density and $d\ell_p$ is an infinitesimal arc length of a poloidal flux contour. We will calculate the three terms separately.

(a) $\int d\ell_p \frac{I(\psi)J_t}{(RB_p)^3}$

$I(\psi)$, $(RB_p)^3$ can be expressed with (ψ,θ) using Eq. (9). J_t should be calculated from the equation

$$J_t = \left(\frac{\partial B_{px}}{\partial z}\right)_R - \left(\frac{\partial B_{pz}}{\partial R}\right)_z \qquad (A.2)$$

$\left(\frac{\partial B_{px}}{\partial z}\right)_R$ and $\left(\frac{\partial B_{pz}}{\partial R}\right)_z$ are transformed to the (ψ,θ) system using the equations

$$\left(\frac{\partial B_{px}}{\partial z}\right)_R = \frac{a' \cos\theta\left(\frac{\partial B_{px}}{\partial \theta}\right)_\psi + a \sin\theta\left(\frac{\partial B_{px}}{\partial \psi}\right)_\theta}{a'b\left(1 + \frac{2e'}{e}\dot{S}a^2 \sin^2\theta + \frac{\delta'}{a'}\cos\theta\right)} \tag{A.3}$$

$$\left(\frac{\partial B_{pz}}{\partial R}\right)_z = \frac{b \cos\theta\left(\frac{\partial B_{pz}}{\partial \psi}\right)_\theta - b' \sin\theta\left(\frac{\partial B_{pz}}{\partial \theta}\right)_\psi}{a'b\left(1 + \frac{2e'}{e}\dot{S}a^2 \sin^2\theta + \frac{\delta'}{a'}\cos\theta\right)} \tag{A.4}$$

B_{px}, B_{pz} can be calculated as functions of (ψ,θ) from the equation $\vec{B}_p = \nabla\zeta \times \nabla\psi$. J_t can be calculated using Eqs. (A.2)-(A.4) straightforwardly. By neglecting terms higher than $O(\varepsilon)$ we get

$$\int d\ell_p \frac{I(\psi)J_t}{(RB_p)^3} = \frac{I(\psi)ae}{(2\dot{S}a)^3}\left[C_1\theta + C_2 \sin 2\theta + C_3\, e \tan^{-1}\left(\frac{1}{e}\tan\theta\right) + C_5 \log\left(\frac{1 + \frac{1}{2e^2} + \sin\theta}{1 + \frac{1}{2e^2} - \sin\theta}\right)\right] \tag{A.5}$$

Here

$$C_1 = \frac{-8\dot{S}^2a^2e'}{R_c e} + \frac{4\dot{S}\dot{S}'a^2}{R_c}$$

$$C_2 = \frac{4\dot{S}^2a^2e'}{R_c e}$$

$$C_3 = \frac{2\dot{S}}{R_c}\left(1 + \frac{1}{e^2} + \frac{4e'\dot{S}a^2}{e}\right) \tag{A.6}$$

$$C_4 = \frac{-2\dot{S}a}{R_c^2}$$

$$\text{(b)} \quad \int d\ell_p \frac{I'(\psi)B_p}{(RB_p)^2}$$

It is straightforward to calculate and the result is

$$\int d\ell_p \frac{B_p I'(\psi)}{(RB_p)^2} = \frac{I'e}{2\dot{S}R_c} \left[\theta\left(1 + \frac{e'}{e}\dot{S}a^2\right) + \left(2\delta'\dot{S}a - \frac{a}{R_c}\right)\sin\theta - \frac{e'\dot{S}a^2}{2e}\sin 2\theta\right] \quad \text{(A.7)}$$

$$\text{(c)} \quad \int d\ell_p \frac{B_p I(\psi)}{(RB_p)^3} \frac{\partial}{\partial\psi}(RB_p)_\chi$$

The calculation of $\frac{\partial}{\partial\psi}(RB_p)_\chi$ can be done in the (ψ,θ) coordinate system using the relations

$$\frac{\partial}{\partial\psi}(RB_p)_\chi = \frac{\partial}{\partial\psi}(RB_p)\Big|_\theta + \frac{\partial}{\partial\theta}(RB_p)\Big|_\psi \frac{\partial\theta}{\partial\psi}\Big|_\chi \quad \text{(A.8)}$$

and

$$\frac{\partial\theta}{\partial\psi}\Big|_\chi = \frac{\nabla\psi \cdot \nabla\theta}{|\nabla\psi|^2} \quad \text{(A.9)}$$

$\nabla\theta$ can be calculated using Eq. (7) in Section 1.

$$\nabla\theta = \frac{(\delta' + a'\cos\theta)\nabla z - b'\sin\theta\,\nabla R}{a'b\left(1 + \frac{2e'}{e}\dot{S}a^2\sin^2\theta + \frac{\delta'}{a}\cos\theta\right)} \quad \text{(A.10)}$$

The calculations of $\left.\frac{\partial\theta}{\partial\psi}\right|_\chi$ and $\frac{\partial}{\partial\psi}(RB_p)_\chi$ are straightforward using Eqs. (A.8)-(A.10); neglecting terms $0(\varepsilon^2)$, the result is

$$\int d\ell_p \frac{B_p I(\psi)}{(RB_p)^3}\frac{\partial}{\partial\psi}(RB_p)_\chi = D_1\theta + D_2 \sin 2\theta + D_3 \frac{\tan\theta}{1+\frac{1}{e^2}\tan^2\theta}$$

$$+ D_4 e \tan^{-1}\left(\frac{1}{e}\tan\theta\right) + D_5 \log\left(\frac{1+\frac{1}{2e^2}+\sin\theta}{1+\frac{1}{2e^2}-\sin\theta}\right) \quad (A.11)$$

Here

$$D_1 = q\left(\frac{\dot{S}'}{\dot{S}} - \frac{2e'}{e}\right)$$

$$D_2 = \frac{-q}{2}\frac{e'}{e}$$

$$D_3 = \frac{q}{4\dot{S}a^2}\left(1 - \frac{1}{e^2} + \frac{3e'}{e}\dot{S}a^2\right) \quad (A.12)$$

$$D_4 = \frac{q}{2\dot{S}a^2}\left(\frac{1}{2} - \frac{1}{e^2} + \frac{3}{2}\frac{e'}{e}\dot{S}a^2\right)$$

$$D_5 = \frac{-q}{4\dot{S}a}\frac{1}{R_c}$$

From Eqs. (A.5), (A.7), and (A.11) we calculate

$$\int\left(\frac{\partial\nu}{\partial\psi}\right)_\chi d\chi$$

The result is

$$\int \left(\frac{\partial \nu}{\partial \psi}\right)_{\chi} d\chi = S_1\theta + S_2 \frac{\tan\theta}{1 + (1/e^2)\tan^2\theta} + S_3 \sin\theta + S_4 \sin 2\theta + S_5\, e \tan^{-1}\left(\frac{1}{e}\tan\theta\right) \qquad \text{(A.13)}$$

Here

$$\begin{aligned} S_1 &= q' \\ S_2 &= \frac{1}{2\dot{S}a^2}\left(1 - \frac{1}{e^2} + \frac{3e'}{e}\dot{S}a^2\right) \\ S_3 &= q'(2\delta'\dot{S}a - a/R_c) \\ S_4 &= \frac{2e'}{e} - \frac{e'}{2e}\dot{S}a^2\left(\frac{q'}{q}\right) \\ S_5 &= \frac{q}{2\dot{S}a^2}\left(\frac{3}{e^2}\right) \end{aligned} \qquad \text{(A.14)}$$

In this calculation we neglect terms with $O(\varepsilon^2)$.

REFERENCES

1. DOBROTT, D., NELSON, D. B., GREENE, J. M., GLASSER, A. H., CHANCE, M. S., FRIEMAN, E. A., Phys. Rev. Lett. 39 (1977) 943.
2. CONNOR, J. W., HASTIE, R. J., TAYLOR, J. B., Phys. Rev. Lett. 40 (1978) 396.
3. GRIMM, R. C., GREENE, J. M., JOHNSON, J. L., Methods in Computational Physics, Vol. 16 (KILLEEN, J., Ed.), Academic Press, New York (1976) 253.
4. BERGER, D., BERNARD, L. C., GRUBER, R., TROYON, F., Plasma Physics and Controlled Nuclear Fusion Research (Proc. 6th Int. Conf. Berchtesgaden, 1976) Vol. 2, IAEA, Vienna (1977) 411.
5. BATEMAN, G., SCHNEIDER, W., GROSSMANN, W., Nucl. Fusion 14 (1974) 669.
6. HICKS, H. R., WOOTEN, J. W., Comput. Phys. Commun. 13 (1977) 117.
7. CLARKE, J. F., SIGMAR, D. J. Phys. Rev. Lett. 38 (1977) 70.
8. MIZOGUCHI, T., KAMMASH, T., SIGMAR, D. J., Phys. Fluids 21 (1978) 2086.
9. GREENE, J. M., JOHNSON, J. L., Plasma Phys. 10 (1968) 729.
10. RUTHERFORD, P. H., CHEN, L., ROSENBLUTH, M. N., Princeton Plasma Physics Laboratory Rep. PPPL-1418 (February 1978).
11. GREENE, J. M., JOHNSON, J. L., Phys. Fluids 5 (1962) 510.
12. BATEMAN, G., MHD Instabilities, M.I.T. Press, Cambridge, Massachusetts, and London, England (1978) 125.
13. BERNSTEIN, I. B., FRIEMAN, E. A., KRUSKAL, M. D., KULSRUD, R. M., Proc. R. Soc. 244A (1958) 17.
14. MERCIER, C., Nucl. Fusion 1 (1960) 47.
15. SOLOV'EV, L. S., Sov. Phys.-JETP 26 (1978) 400.

FIGURE CAPTIONS

FIG. 1. An elliptically elongated poloidal flux surface ψ shifted as $\delta(\psi)$ from the geometric center of the plasma cross section. $a(\psi)$, $b(\psi)$ are minor and major radii of the elliptic surface ψ. R_c is a distance from the axis of the torus to the geometric center of the plasma cross section.

FIG. 2. Eigenfunctions with different shears for the integration angle three and one-half times around the cross section. (a) with high shear; (b) with low shear, plotted with respect to arc length of a poloidal flux surface ψ. The elongation of the plasma edge is $(b/a)w = 3$.

FIG. 3. Eigenfunctions for the integration angle one-half time around the cross section. (a) with high shear; (b) with low shear.

FIG. 4. An angle α between a field line on an elliptically elongated cylindrical flux surface ψ and the z-axis.

FIG. 5. Two adjacent elliptic flux surfaces $\psi - \delta\psi$ and ψ. A generalized poloidal angle χ is determined exactly the same as an elliptic angle θ on the flux surface $\psi - \delta\psi$. The deviation of these two angles is shown in the flux surface ψ.

FIG. 6. The relations between χ and θ on two adjacent flux surfaces $\psi - \delta\psi$ and ψ.

FIG. 7. Marginal beta as functions of β_p for different shear with same pressure profile $p(\psi) = A\psi^2$, elongation $(b/a)w = 3$.

FIG. 8. Marginal beta as functions of β_p for different aspect ratio ASP = 3, 4, 5 with $q(\psi) = A - 2\psi$, $p(\psi) = B\psi^2$, $(b/a)w = 3$.

FIG. 9. Marginal beta as functions of β_p for different breadth of pressure profile. ASP = 4, (b/a)w = 3, and $q(\psi) = A - 2\psi$.

FIG. 10. Convergence study with different integration angle. Solid lines are with $q_a = 1$ and dotted lines are with $q_a = 1.5$.

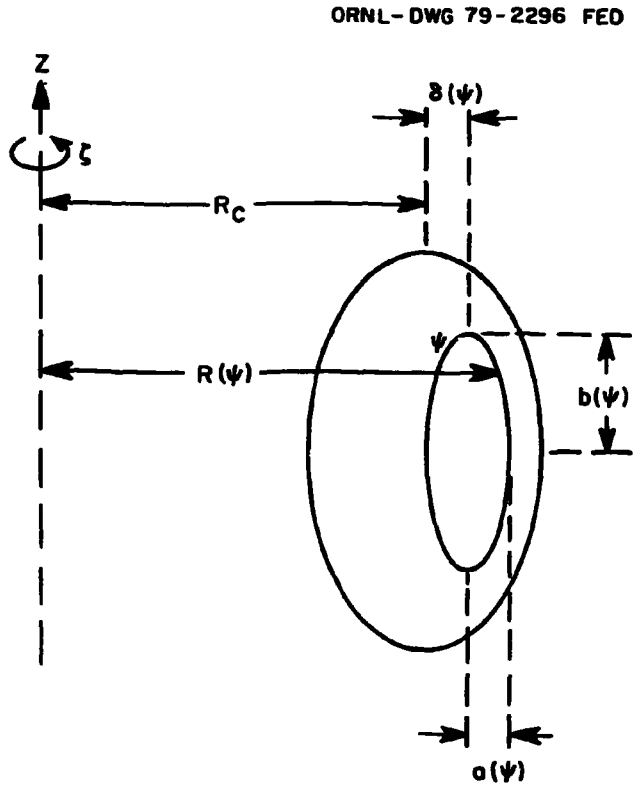

Fig. 1.

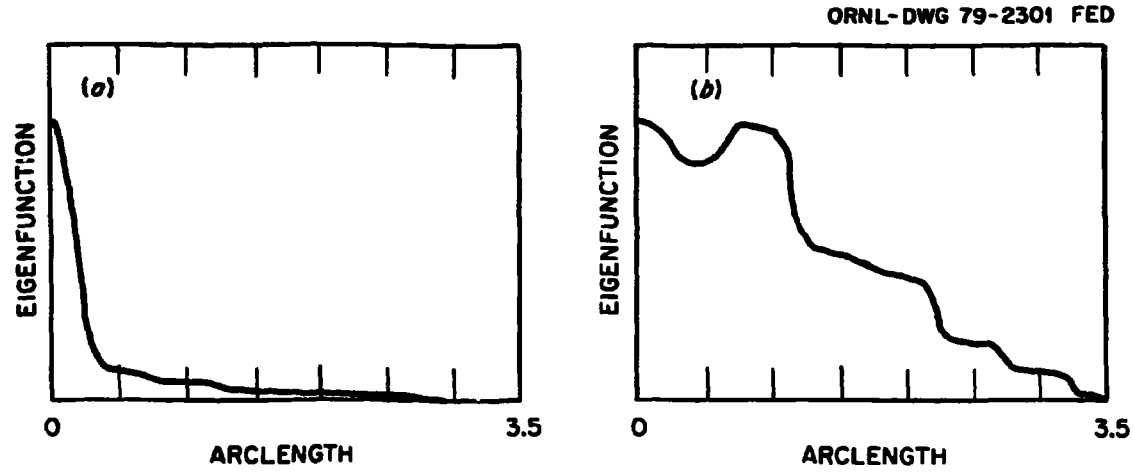
ORNL-DWG 79-2301 FED
(a)
(b)
EIGENFUNCTION
EIGENFUNCTION
0
3.5
0
3.5
ARCLENGTH
ARCLENGTH

Fig. 2.

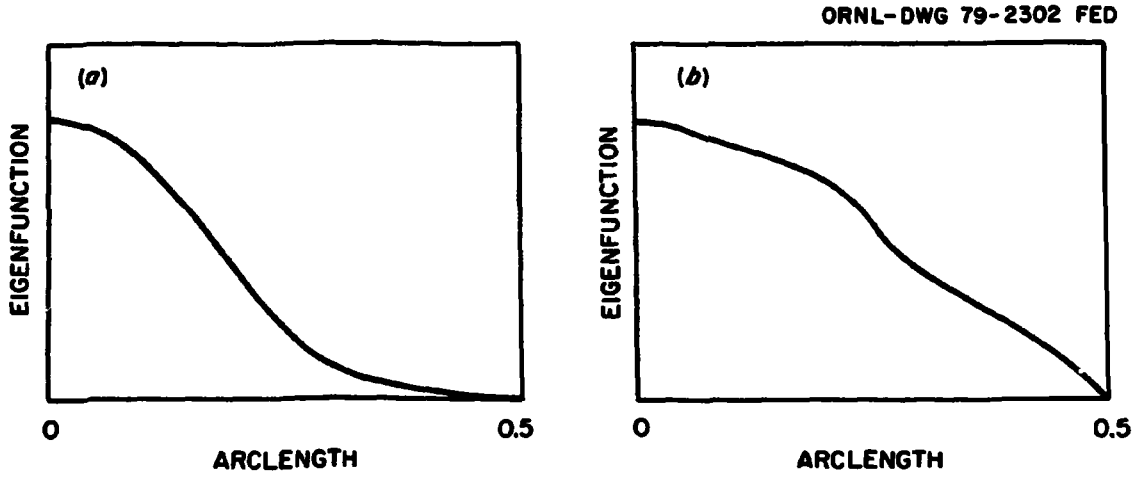
ORNL-DWG 79-2302 FED
(a)
(b)
EIGENFUNCTION
EIGENFUNCTION
0
0.5
0
0.5
ARCLENGTH
ARCLENGTH

Fig. 3.

ORNL-DWG 79-2297 FED

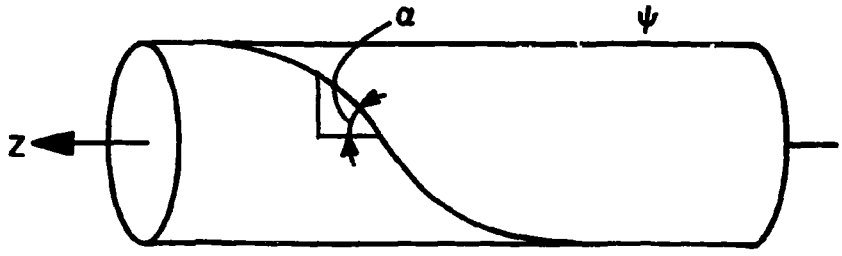

Fig. 4.

ORNL-DWG 79-2298 FED

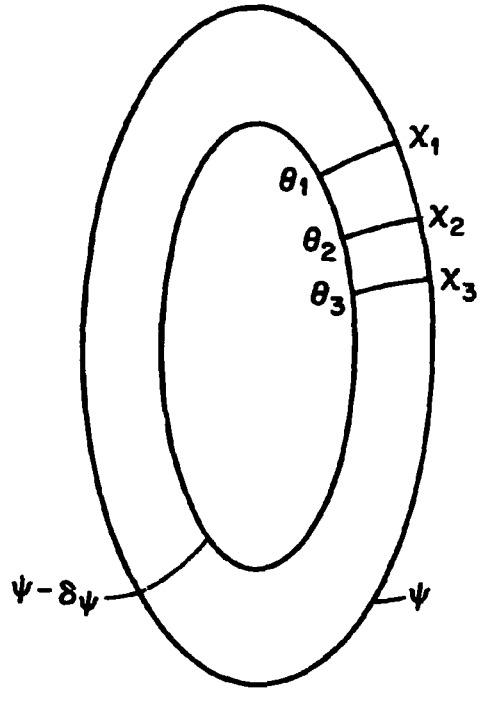

Fig. 5.

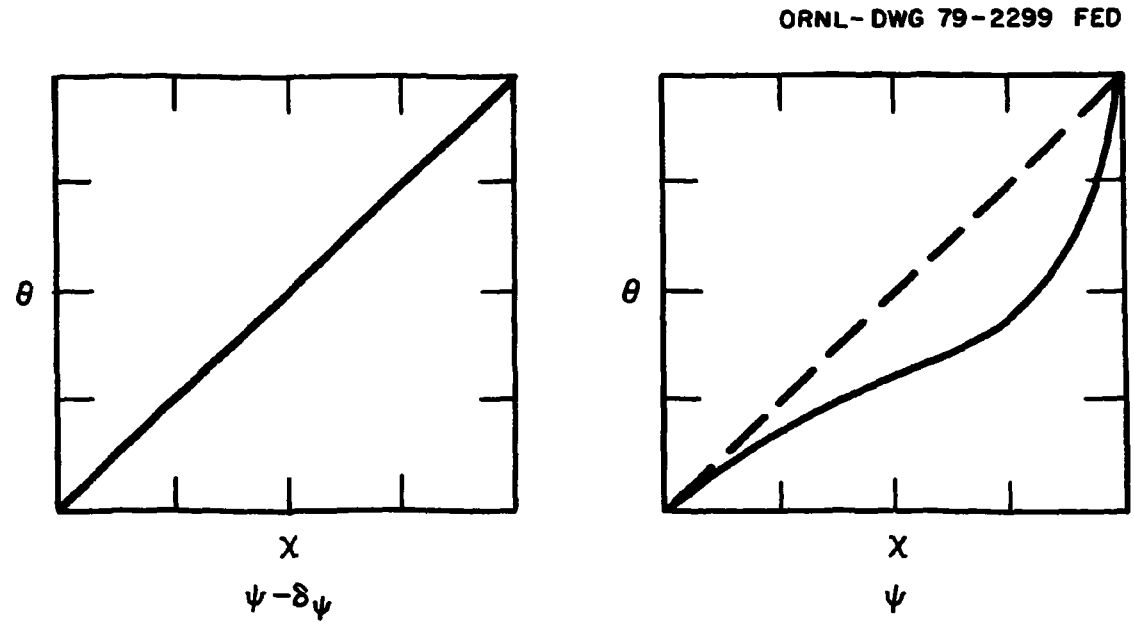

Fig. 6.

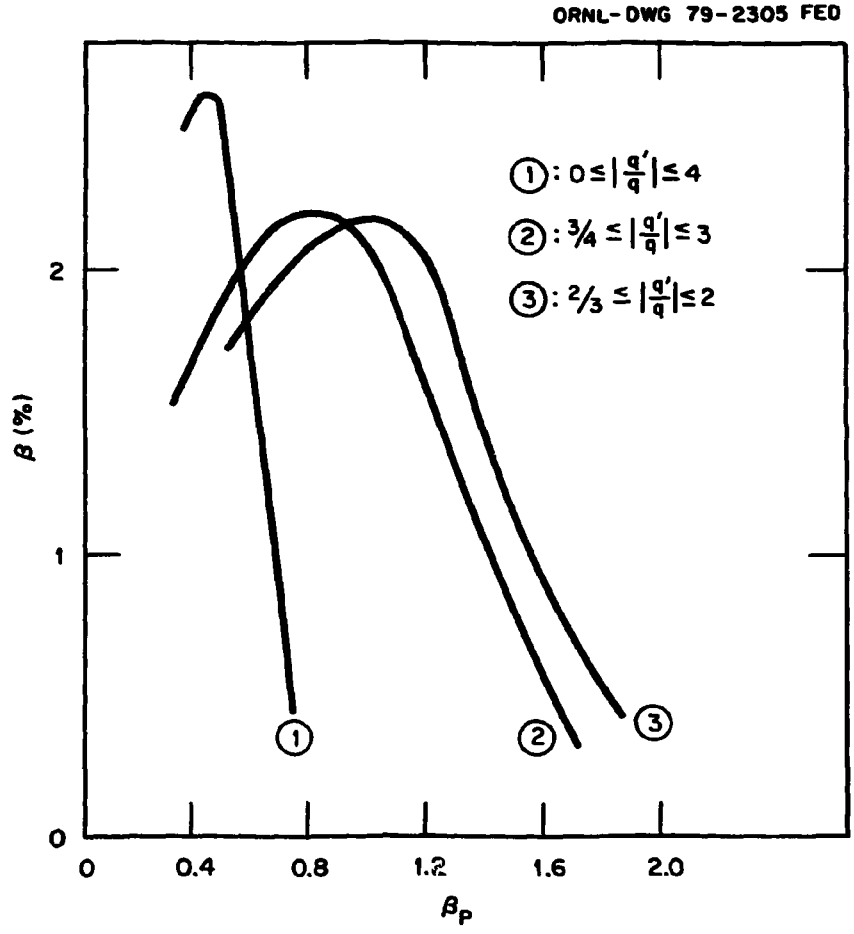
ORNL-DWG 79-2305 FED
①: 0 ≤ |q'/q| ≤ 4
②: 3/4 ≤ |q'/q| ≤ 3
③: 2/3 ≤ |q'/q| ≤ 2
β (%)
0
1
2
0
0.4
0.8
1.2
1.6
2.0
β_P

Fig. 7.

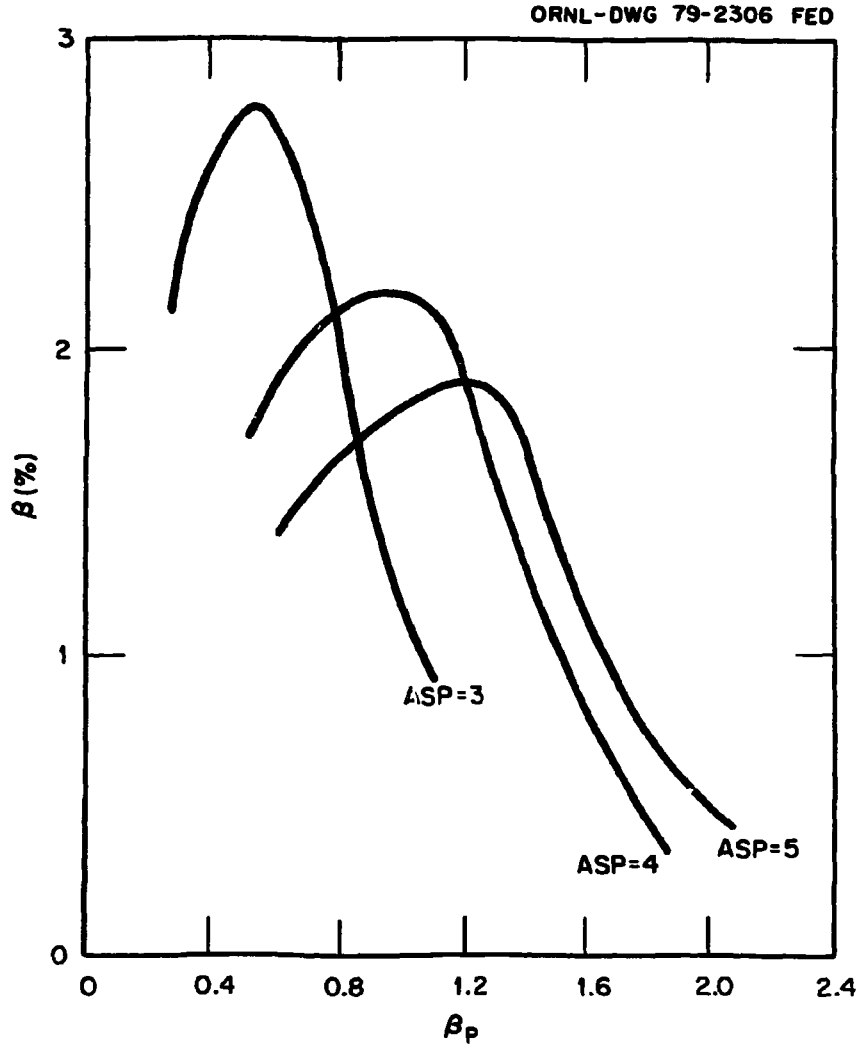

Fig. 8.

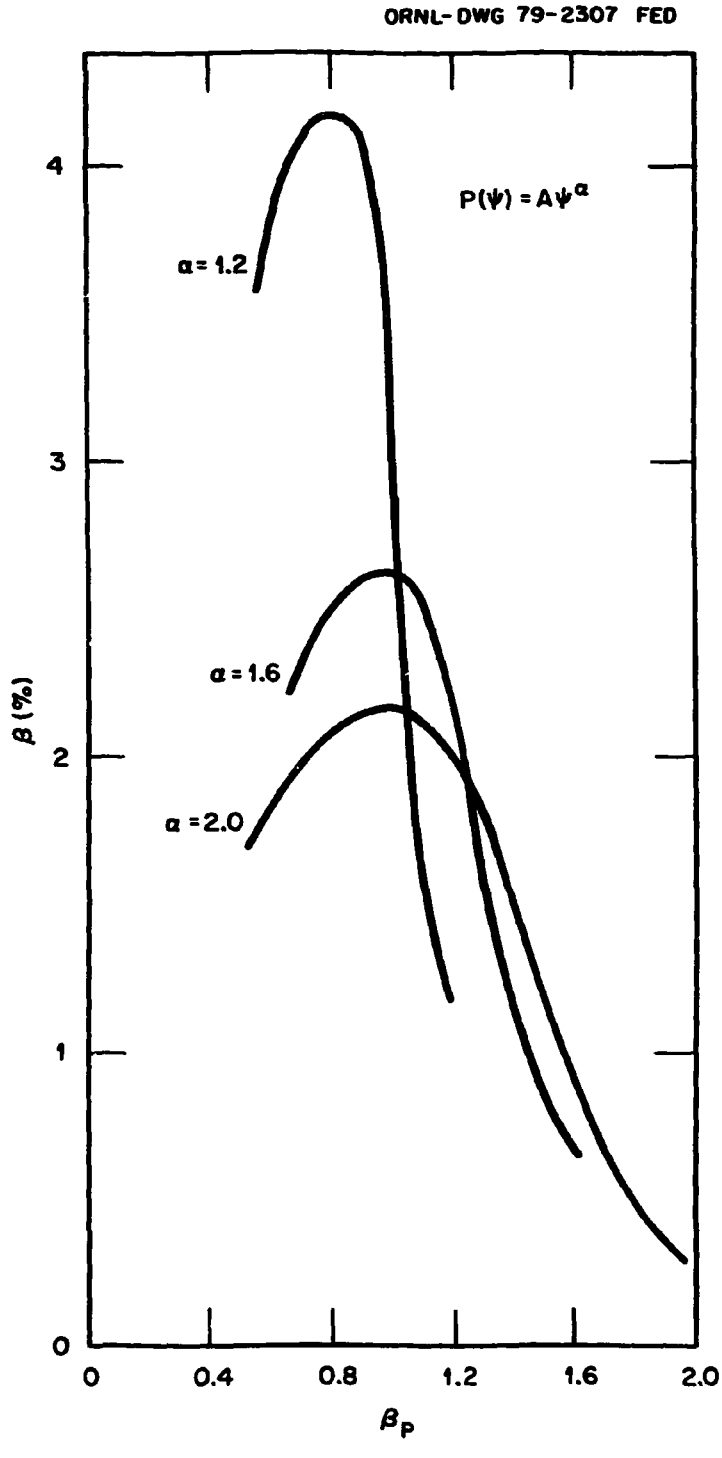

Fig. 9.

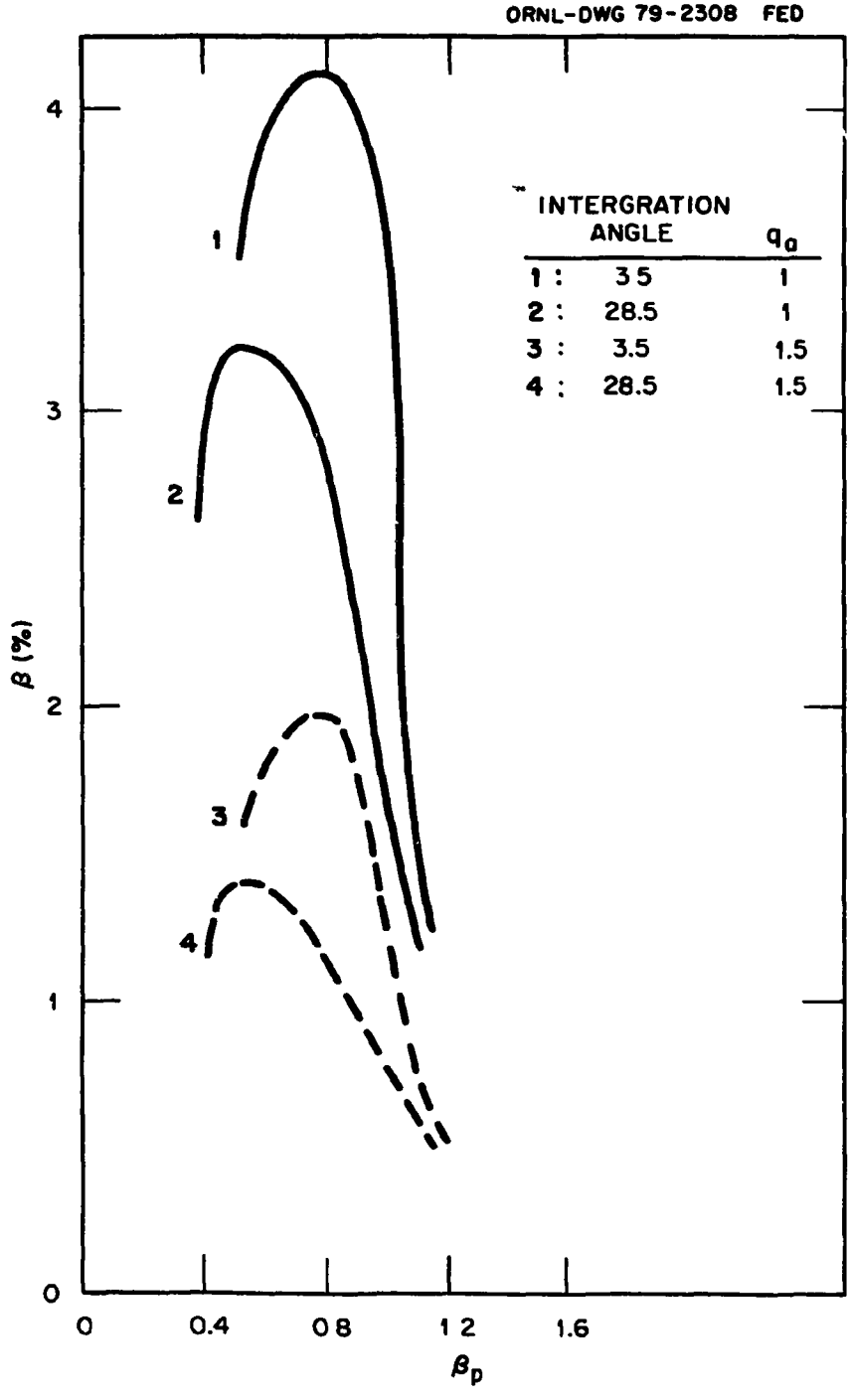
ORNL-DWG 79-2308 FED
INTERGRATION ANGLE
q_a
1 : 35 1
2 : 28.5 1
3 : 3.5 1.5
4 : 28.5 1.5
1
2
3
4
β (%)
0
1
2
3
4
0
0.4
0.8
1.2
1.6
β_p

Fig. 10.